ENGINEERING TRANSACTIONS • *Engng. Trans.* • **62**, 3, 221–240, 2014
Polish Academy of Sciences • Institute of Fundamental Technological Research (IPPT PAN)
National Engineering School of Metz (ENIM) • Poznan University of Technology

The Identfication Procedure for The Constitutive Model of Elasto-Viscoplasticity Describing the Behaviour of Nanocrystalline Titanium

Zdzisław NOWAK, Piotr PERZYNA

Department of Mechanics of Materials
Institute of Fundamental Technological Research
Polish Academy of Sciences
Pawińskiego 5B, 02-106 Warszawa, Poland
e-mail: znowak@ippt.pan.pl

The main objective of the present paper is the description of the behaviour of the ultrafine-grained (UFG) titanium by the constitutive model of elasto-viscoplasticity with the development of the identification procedure. We intend to utilize the constitutive model of the thermodynamical theory of elasto-viscoplasticity for description of nanocrystalline metals presented by Perzyna [21]. The identification procedure is based on experimental observation data obtained by Jia *et al.* [11] for ultrafine-grained titanium and by Wang *et al.* [25] for nanostructured titanium. Hexagonal close-packed (hcp) ultrafine-grained titanium processed by sever plastic deformation (SPD) has gained wide interest due to its excellent mechanical properties and potential applications as biomedical implants.

Key words: elasto-viscoplasticity, nanocrystalline titanium, uniaxial compression.

1. Prologue

The main objective of the present paper is the development of identification procedure of the constitutive model of elasto-viscoplasticity describing the behaviour of nanocrystalline titanium. An investigating of the deformation mechanisms is important for understanding, controlling and optimizing the mechanical properties of nanocrystalline metals. Strengthening with grain size refinement in metals and alloys with an average grain size of 100 nm or larger has been well characterized by the Hall-Petch (H-P) relationship, where dislocation pile-up against grain boundaries along with other transgranular dislocations mechanisms are the dominant strength-controlling processes. When the average, and entire range of, grain sizes is reduced to less than 100 nm, the dislocation opera-

tion becomes increasingly more difficult and grain boundary-mediated processes become increasingly more important, cf. MEYERS [13].

Titanium and titanium alloys constitute an important class of metals with many commercial applications in the defence, aerospace, biomedical, and sporting goods industries. Pure titanium has a hexagonal close-packed structure. The polycrystalline titanium is observed to be ductile in a wide range of testing conditions and it is generally assumed that the above slip mechanisms are augmented by slip and/or deformation twinning, cf. CHRISTIAN and MAHAJAN [4] and GURAO *et al.* [10]. WANG *et al.* [25] attributed the higher hardening rates in the large grain sized high-purity Ti to deformation twins acting as barriers to slip via a Hall-Petch type hardening mechanism. WANG *et al.* [25] indicate that deformation twinning in high-purity Ti does indeed play an important role in the strain hardening response of this metal. In another study, NEMAT-NASSER *et al.* [14], reported three stages of hardening in the stress-strain curves during plastic deformation of polycrystalline commercially pure titanium at various strain rates and temperatures. They labelled these three stages as stage-I with a decreasing slope of the stress-strain curve, followed by stage-II with an increasing slope, then stage-III again with a decreasing slope. Previous studies in *fcc* alloys deformed at room temperature, cf. EL-DANAF *et al.* [9] had concluded that such similar changes in strain hardening rates were associated with deformation twinning. In another study, SALEM *et al.* [24] reported the changes in microstructure evolution in high purity α-Titanium and correlating them to distinct changes in strain hardening response of the material. The work by SALEM *et al.* [24] provide a comparison of the strain hardening responses of *fcc* metals and *hcp* metals when deformation twinning is a prevalent mechanism. The principal short-range barrier, the Peierls-Nabarro stress, is important for ultrafine crystalline *bcc* metals. Experimental observations have shown that nanosized grains rotate during plastic deformation and can coalesce along directions of shear, creating larger paths for dislocation movement.

Many results have shown that nanocrystalline materials exhibit the grain size and strain rate dependent mechanical behaviors, the relative review can be seen in MAYERS *et al.* [13]. To understand this sort of mechanical behaviour, several models have been proposed recently using the concept of a two-phase composite. ZHU *et al.* [29] developed a polycrystalline constitutive theory based on the model of ASARO *et al.* [1] for deformation mechanisms in nanocrystalline metals and the extended aggregate Taylor model by ASARO and NEEDLEMAN [2]. Despite the successes provided by these models, the effects of grain size and strain rate (especially in a wide strain rate range) on the mechanical behaviour of nanocrystalline materials are not well described in term of their main deformation mechanisms as yet. The deformation mechanism of the nanocrystalline

material is very complicated. Even for the same material, the deformation mechanism will also change with the further deformation. For example, the shear band evolution phenomena during the inelastic deformation process have been observed in the compression tests by WANG *et al.* [25], this indicates that the deformation will become non-uniform in the deformation process.

In this paper, we will be focused on the description of the behaviour of nanocrystalline titanium in viscoplastic strain range. The viscoplasticity model proposed by PERZYNA [21] will be used to simulate the grain size and strain rate dependent mechanical behaviour of *hcp* nanocrystalline materials, and the numerical simulation results for *hcp* nanocrystalline materials will be compared with JIA *et al.* [11] and WANG *et al.* [25] experimental data for titanium. Finally, further discussion will be presented for the uniaxial stress-strain response, shear localization behaviours and strain rate sensitivity of *hcp* nanocrystalline metal.

2. Experimental observations

Main experimental observations for constitutive modeling during plastic deformation of nc-Ti, Ultrafine-grained Ti was produced by equal channel angular pressing (ECAP) of commercial purity titanium (0.12%O, 0.07%C, 0.04%N, 0.01%H, 0.18%Fe, and balanced Ti) following route Bc for eight passes at 400–450°C. In the paper (cf. WANG *et al.* [25–27]) extended the mechanical testing of nanostructured Ti to much larger strains and a wide range of strain rates in order to understand what factors and how they control the deformation/failure behaviour of UFG-Ti. They paid special attention on the possibility of twinning activities in nanostructured Ti that were previously overlooked. In order to do so, the mechanical properties of commercial purity nanostructured titanium prepared by equal channel angular pressing plus cold rolling (grain size ~ 260 nm) were systematically characterized. Hexagonal close-packed (*hcp*) ultrafine-grained (UFG) titanium processed by sever plastic deformation (SPD) has gained wide interest due to its excellent mechanical properties and potential applications as biomedical implants.

It is well-established that deformation twinning is an important mode of deformation in coarse-grained (CG) *hcp* materials. Experimental observations confirmed that the nanostructured titanium prepared by SPD contains not only high densities of dislocations but also a significant amount of deformation twins. Such unique microstructural characteristic suggests that the deformation mechanism and failure mode of nanostructured Ti may be different from those of other UFG materials.

Figure 1a shows true stress-strain curves of UFG-Ti with the strain rate in the range of $10^{-4} - 10^{-1}$ s^{-1}. For comparison, the stress-strain curve of a CG-Ti (grain size ~ 35 μm) is also included.

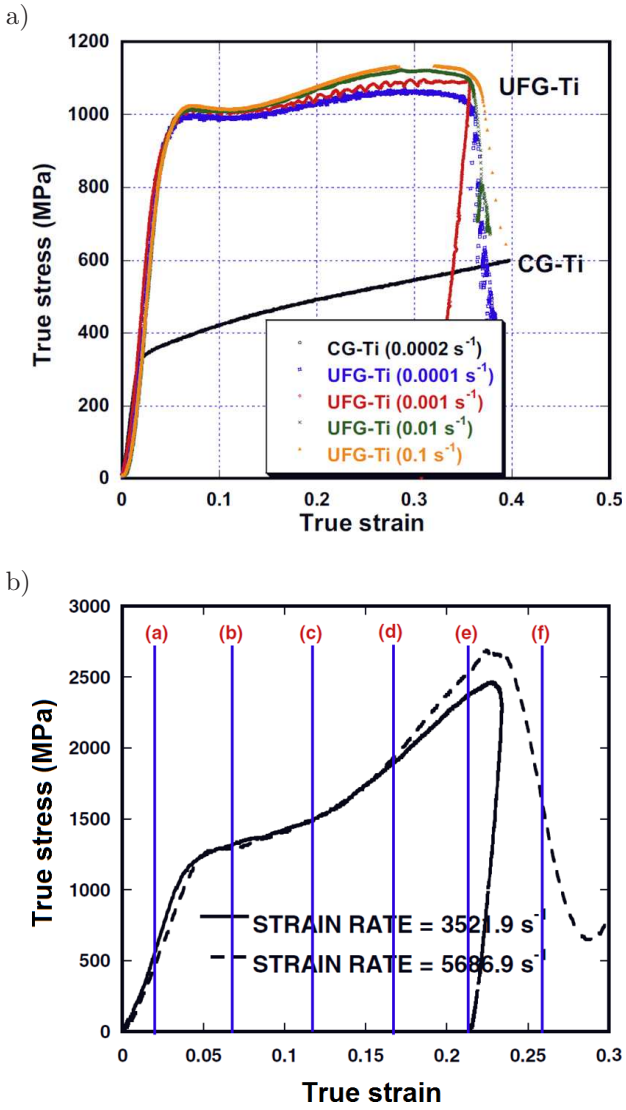

FIG. 1. a) Typical compression true stress-strain curves obtained for UFG-Ti at a room temperature quasistatic-strain rate ($1\times10^{-4}-1\times10^{-1}$ s^{-1}); b) high-strain-rate ($3.5–5.68\times10^{+3}$ s^{-1}), with a curve for CG-Ti for comparison are shown; experimental data of WANG *et al.* [25].

A considerably elevated strength was observed in UFG-Ti with the yield stress 3–4 times higher than that of CG-Ti. In terms of ductility, UFG-Ti fails after a total compressive strain of ∼30%, as compared to ∼60% in CGTi. Careful examinations of the strain hardening behaviour in UFG-Ti and CG-Ti reveal distinctive differences. The CG-Ti demonstrates a strong strain hardening behaviour throughout the test. Such an increasing strain hardening behaviour in

CG-Ti is believed to be associated with extensive twinning. In contrast, a different scenario is observed for the plastic flow of UFG-Ti, which exhibits initially strain hardening, with a near perfectly plastic behaviour at strain up to 15%. This is strain hardening behaviour at small strain agrees with previous observations (cf. Jia *et al.* [11]) and is believed to render tensile instability in nanostructured Ti. At large strains, however, a no negligible strain hardening is observed. The strain hardening for UFG-Ti becomes more pronounced when the samples were tested at high strain rates, as shown in Fig. 1b.

Figure 2 displayed sequential TEM bright field images of the as-processed and deformed UFG-Ti. Due to the cold-rolling procedure, many grains in the

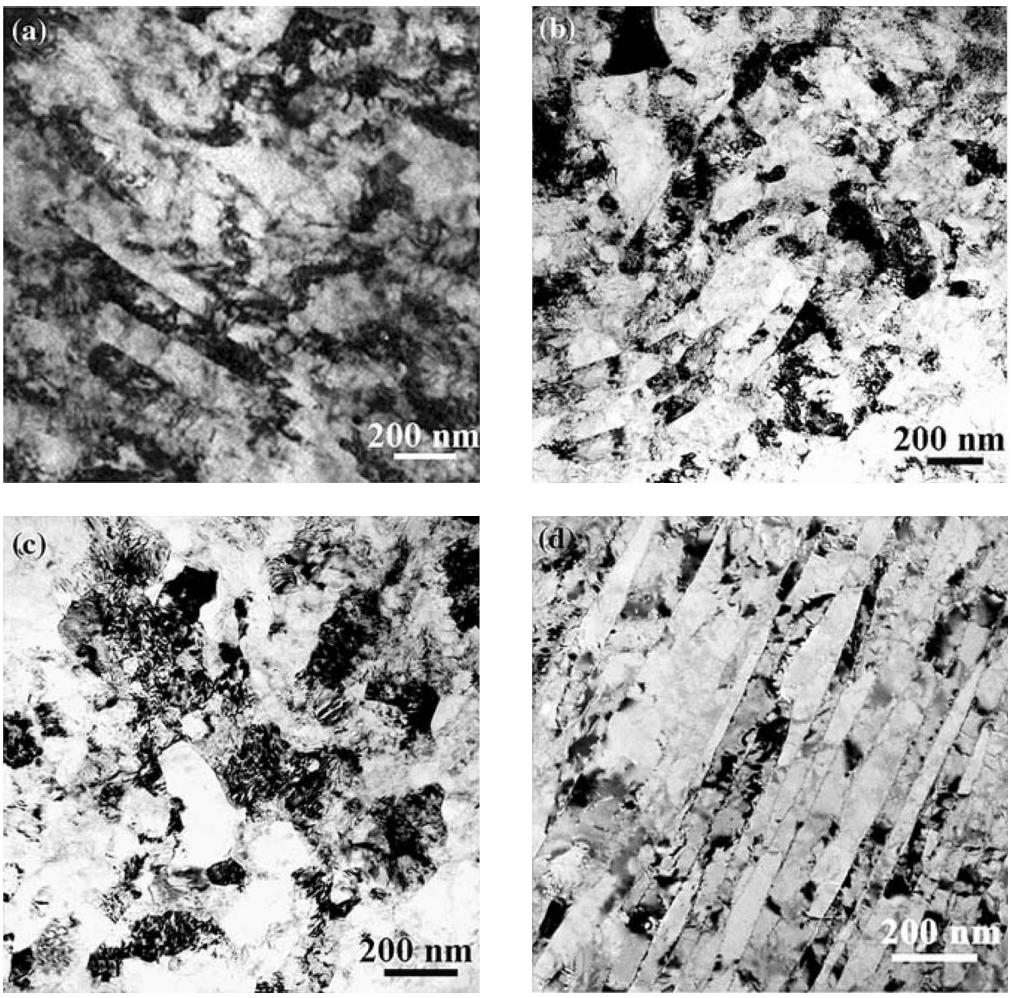

Fig. 2. TEM bright-field images of: a) as-processed (an average grain size of ∼260 nm), b) 8% deformed UFG-Ti, c) 30% deformed (the grains look completely equal-axed) and d) high strain rate deformed UFG-Ti (the band width in the range of 50–100 nm); from Wang *et al.* [25].

as-prepared samples exhibit filamentary shape along the longitudinal rolling direction (Fig. 2a), with an average grain size of ∼260 nm.

Dislocation cells and extremely high density of dislocations are the typical microstructural features. Deformation twins resulted from severe plastic deformation are also visible inside grains with the twin band width on the order of ∼150 nm. After 10% deformation (Fig. 2b), the ultra-fine-grains become more or less equiaxed, though some grains with straight boundaries and elongated contours are still observable. The average grain size remains approximate constant across the transverse direction. After 30% strain (Fig. 2c), the grains look completely equal-axed (the sample failed at this point). The transformation dislocation slip plays a significant role during plastic deformation of UFG-Ti. TEM examinations in quasi-static deformed samples supports the notion that dislocation slip is the major deformation in nanostructured Ti at slow deformation and room temperature (cf. Zhu *et al.* [30]).

At dynamic loading rates ($10^3 - 10^4$ s^{-1}), however, a different scenario is observed (Fig. 2d). Deformation twin with the band width in the range of 50–100 nm become the characteristic microstructural feature. The twin bands in as-processed samples are noticeable wider, suggesting that deformation twinning has become an important event high strain rate deformation of UFG-Ti. Extensive twinning activities were also observed when nanostructured Ti was deformed at cryogenic temperature (77 K, cf. Wang *et al.* [28]. The twin bands observed in low temperature deformation is narrower (in the range of 10–50 nm) than those seen at high strain rates. This indicates that the twinning activity in nanostructured Ti is closely tied to deformation conditions such as strain rates and temperature.

Jia *et al.* [11] investigated deformation behaviour and plastic instabilities of ultrafine-grained titanium. Figure 3 shows a true stress-strain curve for the as-processed UFG-Ti in comparison with that for the CG-Ti, obtained uniaxial compression at 2×10^{-4} s^{-1}. At a strain of 6% the flow stress of the UFG-Ti (1.02 GPa) is more than twice that of CG-Ti (0.45 GPa), consistent with the Hall-Patch relationship for conventional Ti. The as-processed UFG-Ti exhibits little strain hardening, with a nearly perfectly plastic behaviour at strain above 5%. In comparison, CG-Ti shows obvious strain hardening. The stress-strain curve for UFG-Ti after annealing is also included in Fig. 3.

Compared with the as-processed case, the yield strength of the annealed UFG-Ti is lower. The strain-hardening rate, on the other hand, is higher than the as-processed case for strains less than ∼5%, which is attributable to the recovery of the cold-worked grains. However, due to the small grain size, the capacity for the accumulation of dislocations and twin boundaries and hence strain hardening remains very limited and far less than that of CG-Ti. The higher strain hardening of the annealed UFG-Ti would also help overcome soft-

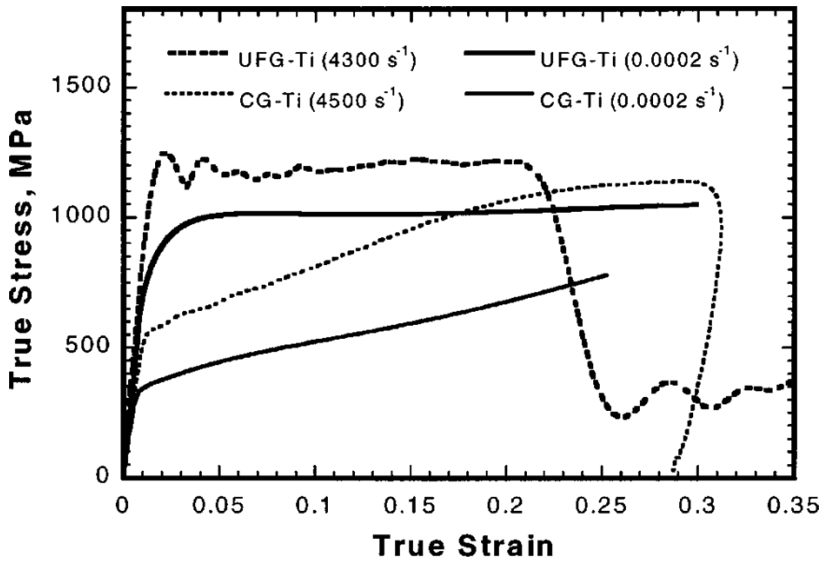

FIG. 3. Comparison of high-strain-rate true stress-strain curves with those at quasistatic-strain rates for both the annealed UFG-Ti and CG-Ti. Experimental data of JIA *et al.* [11].

ening caused by flaws or damage sites operative in tension. The strain-rates dependence of the flow stress at a constant strain 6% is plotted in Fig. 4 for the strain-rate range from 2×10^{-4} to 9×10^{-4} s^{-1}. If a linear relationship is assumed,

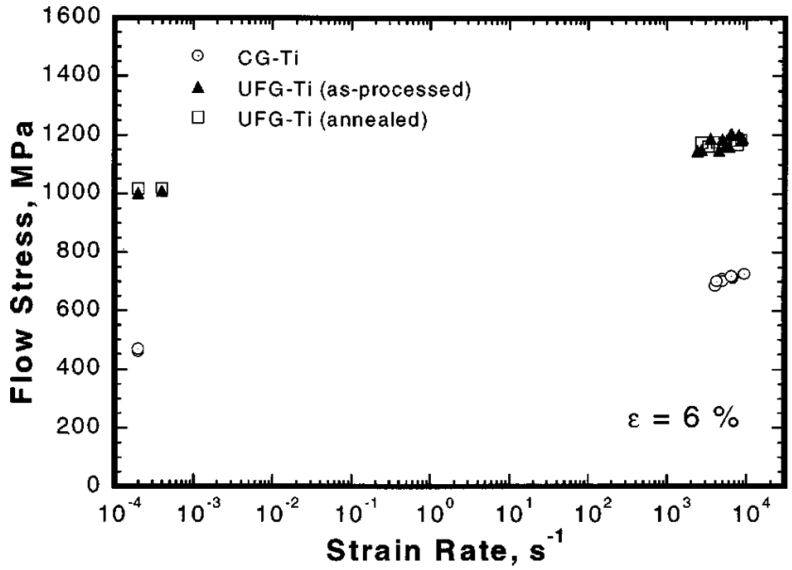

FIG. 4. Strain-rate dependence of the flow stress of UFG-Ti and CG-Ti at a strain of 6%. Experimental data of JIA *et al.* [11].

the UFG-Ti lines have similar slopes $(\partial\sigma/\log\dot{\in}) \in$, indicating that he magnitude of the strain-rate enhancement of the flow stress (∼200 MPa) is similar for these two very different grain sizes.

Experimental observation for nc-Ti base on paper by JIA *et al.* [11], NEMAT-NASSER *et al.* [14] and WANG *et al.* [25] can be summarize for *hcp* materials as follows:

(i) the deformation mode of nc-Ti changes dramatically as the grain size is decreased into the ultrafine and nano grain range;

(ii) for all grain sizes $d > 300$ nm, deformation of Ti were uniform at all strain rates;

(iii) for all smaller grain sizes $d < 300$ nm shear bands were observed during both quasistatic and high rate deformation.

3. The constitutive model

3.1. The thermo-elasto-viscoplastic relations

We propose to introduce some simplification of the constitutive model developed by PERZYNA [21] by assuming that the internal state variable vector $\boldsymbol{\mu} = (\in^p, d, \boldsymbol{\xi})$ consists of two scalars and one tensor, i.e. $\in^p$ denotes the equivalent viscoplastic deformation, d defines the mean grain diameter and $\boldsymbol{\xi}$ is the microdamage second order tensor, with the physical interpretation that $(\boldsymbol{\xi} : \boldsymbol{\xi})^{1/2} = \xi$ defines the volume fraction porosity. The equivalent inelastic deformation $\in^p$ describes the dissipation effects generated by viscoplastic flow phenomena, the microdamage tensor $\boldsymbol{\xi}$ takes into account the anisotropic intrinsic microdamage mechanisms on internal dissipation and d describes the dynamic grain growth during intensive deformation process.

We postulate the plastic potential function in the form $f = f(J_1, J_2, \vartheta, \boldsymbol{\mu})$, where J_1, J_2 denote the first two invariants of the Kirchhoff stress tensor $\boldsymbol{\tau}$ and ϑ is absolute temperature. The evolution equations are assumed as follows

$$\mathbf{d}^p = \Lambda\mathbf{P}, \qquad \mathrm{L}_{\upsilon}\boldsymbol{\xi} = \boldsymbol{\Xi}, \qquad \dot{d} = D, \tag{3.1}$$

where

$$\Lambda = \frac{1}{T_m}\left\langle \Phi\left(\frac{f}{\kappa} - 1\right)\right\rangle, \qquad \mathbf{P} = \left.\frac{\partial f}{\partial \boldsymbol{\tau}}\right|_{\boldsymbol{\xi}=\mathrm{const}} \left(\left\|\frac{\partial f}{\partial \boldsymbol{\tau}}\right\|\right)^{-1}, \tag{3.2}$$

$\mathbf{d}^p$ denotes the rate of inelastic deformation tensor, T_m denotes the relaxation time for mechanical disturbances, the isotropic work-hardening-softening func-

tion $\kappa = \widehat{\kappa}(\in^p, \vartheta, \boldsymbol{\xi}, d)$, Φ is the empirical overstress function, the bracket $\langle\cdot\rangle$ defines the ramp function, $\mathrm{L}_{\boldsymbol{\upsilon}}$ denotes the Lie derivative and $\boldsymbol{\Xi}$ and D denote the evolution functions which have to be determined.

Let us assume that the intrinsic microdamage process is generated by growth mechanism only. Based on the heuristic suggestions and taking into account the influence of the stress triaxiality and anisotropic effects on the growth mechanism we assume the evolution equation for the microdamage tensor $\boldsymbol{\xi}$ as follows

$$\mathrm{L}_{\boldsymbol{\upsilon}}\boldsymbol{\xi} = \frac{\partial g^*}{\partial \boldsymbol{\tau}} \frac{1}{T_m} \left\langle \Phi\left[\frac{I_g}{\tau_{eq}(\vartheta, \boldsymbol{\mu})} - 1\right]\right\rangle. \tag{3.3}$$

The tensorial function $\partial g^*/\partial\boldsymbol{\tau}$ represents the mutual micro(nano)crack interaction for growth process, $\tau_{\mathrm{eq}} = \widehat{\tau}(\vartheta, \boldsymbol{\mu})$ denotes the threshold stress function for growth mechanism, $I_g = b_1 J_1 + b_2\sqrt{J_2'}$ defines the stress intensity invariant, J_2' denote the second invariant of the Kirchhoff stress deviator tensor, b_i $(i = 1, 2)$ are the material coefficients which can depend on d. In the evolution Eq. (3.3) the function $g = \widehat{g}$ $(\boldsymbol{\tau}, \vartheta, \boldsymbol{\mu})$ plays the fundamental role, and we introduce the denotation $\dfrac{\partial g^*}{\partial \boldsymbol{\tau}} = \dfrac{\partial \widehat{g}}{\partial \boldsymbol{\tau}} \left(\left|\left|\dfrac{\partial \widehat{g}}{\partial \boldsymbol{\tau}}\right|\right|\right)^{-1}$. Assuming that the dynamic grain growth is the rate dependent mechanism (cf. Perzyna [21]) we postulate

$$\dot{d} = \frac{\widehat{\mathcal{G}}(\vartheta, \boldsymbol{\mu})}{T_m} \left\langle \Phi\left[\frac{I_d}{\tau_d(\vartheta, \boldsymbol{\mu})} - 1\right]\right\rangle, \tag{3.4}$$

where $\mathcal{G} = \widehat{\mathcal{G}}(\vartheta, \boldsymbol{\mu})$ is the material function, $I_d = c_1 J_1 + c_2\sqrt{J_2'}$ represents the stress intensity invariant for grain growth, c_i $(i = 1, 2)$ are the material coefficients which may depend on d, and $\tau_d = \widehat{\tau}_d(\vartheta, \boldsymbol{\mu})$ denotes the threshold stress for dynamic grain growth mechanism. For previous theoretical and experimental works on this problem please consider following papers, e.g. Chen *et al.* [3], Kumar *et al.* [12], Meyers *et al.* [13] and Nowak and Perzyna [15].

4. The identification procedure

The identification procedure consists of two parts. In the first part the determination of the material functions and the material constants involved in the description of the dynamic yield criterion (4.3) is presented. As an experimental base the results concerning a set of stress-strain responses of the consolidated iron obtained from the quasistatic compression tests and at high strain rates

$(3 \times 10^3 - 6 \times 10^3\ \mathrm{s}^{-1})$ for several grain sizes by JIA *et al.* [11]. The second part is the identification focused on the determination of the material functions and the material constants appeared in the evolution Eqs. (3.3) and (3.4). However, before our final approach to the identification of all parameters of our model, we assume that the grain size is constant, function $\mathcal{G} = 0$ in Eq. (3.4). Let us also assume that for simplicity we use the scalar internal state variable $\xi = (\boldsymbol{\xi} : \boldsymbol{\xi})^{1/2}$ instead of microdamage tensor $\boldsymbol{\xi}$ and we propose the evolution equation for the porosity ξ as follows (cf. PERZYNA [18])

$$\dot{\xi} = \dot{\xi}_{\mathrm{grow}} = \frac{g^*(\xi, \vartheta)}{T_m \kappa_0(\vartheta)} \left[I_g - \tau_{\mathrm{eq}}(\xi, \vartheta, \in^p) \right], \tag{4.1}$$

where $T_m \kappa_0(\vartheta)$ denotes the dynamical viscosity of a material and $\tau_{\mathrm{eq}}(\xi, \vartheta, \in^p)$ is the void growth threshold stress.

4.1. The determination of the dynamic yield criterion

The plastic potential function f is assumed in the form (cf. PERZYNA [17])

$$f = \left[J_2' + n\,(\vartheta, d)\,(\boldsymbol{\xi} : \boldsymbol{\xi})^{1/2} \left(J_1^2 \right) \right]^{1/2}, \tag{4.2}$$

where J_1 is the first invariant of the Kirchhoff stress $\boldsymbol{\tau}$, J_2' denotes the second invariant of the stress deviator of the Kirchhoff stress $\boldsymbol{\tau}$ and $n = n(\vartheta)$ is the material function. From Eq. $(3.2)_1$, Eq. $(3.2)_2$ and (3.1) we have the dynamical yield criterion in the form

$$\left[J_2' + n\,(\vartheta, d)\,(\boldsymbol{\xi} : \boldsymbol{\xi})^{1/2} \left(J_1^2 \right) \right]^{1/2} = \kappa \left[1 + \Phi^{-1} \left(\frac{\sqrt{3}}{2} T_m \dot{\in}^p \right) \right], \tag{4.3}$$

where $\kappa = \kappa_0(\vartheta) + \kappa^*(\in^p)$ is the isotropic work-hardening-softening function.

In the clasical theory of Perzyna viscoplasticity, cf. PERZYNA [21], the relaxation time T_m governs the viscoplastic flow in the entire range of strain rate changes and can be obtained based on experimental data. It is evident from experimental data for iron PERZYNA [16], that in region of $10^{-3} \leq \dot{\in}^p \leq 10^{+5}\ \mathrm{s}^{-1}$ the relaxation time is not a constant value and can change. One possible idea to include in model such change has been proposed by PERZYNA [16] by introduction the control function, another idea is to include the micro-shear banging effects PERZYNA [21].

Let us assume that T_m depend on the rate of the equivalent plastic strain $\dot{\in}^p$. Taking advantage of the description of the microshear banding effects for nanocrystalline titanium we can propose the relation for the relaxation time T_m proposed by PERZYNA [19–21], PĘCHERSKI [22, 23]]

$$T_m = T_m^0 \left[1 - f_{SB}^0 \frac{1}{1 + \exp\left(a - b \in^p\right)}\right] \left(\frac{\dot{\in}^p}{\dot{\in}_s^p} - 1\right)^{m_2}, \tag{4.4}$$

where T_m^0, m_2, f_{SB}^0, a, b and $\dot{\in}_s^p$ are material functions of d.

4.2. Assumption of the material functions for an adiabatic process

To do the proper identification procedure we first make assumption of the material functions (cf. DORNOWSKI and PERZYNA [6]).

Let us introduce the particular form for the plastic potential function as follows

$$f = \left\{J_2' + \left[n_1(\vartheta) + n_2(\vartheta)\xi\right] J_1^2\right\}^{1/2}. \tag{4.5}$$

where

$$n_1(\vartheta) = 0, \qquad n_2(\vartheta) = n_2 = \text{const}. \tag{4.6}$$

The isotropic work-hardening-softening function κ is postulated as

$$\kappa = \widehat{\kappa}(\in^p, \vartheta, \xi) = \left[A + B(\in^p)^n\right]. \tag{4.7}$$

The overstress function $\Phi\left(\dfrac{f}{\kappa} - 1\right)$ is assumed in the form

$$\Phi\left(\frac{f}{\kappa} - 1\right) = \left(\frac{f}{\kappa} - 1\right)^{1/q}, \tag{4.8}$$

where q is material constant and for Ti we assume $1/q = m_2$ (cf. Eq. (4.4)).

4.3. The determination of the material functions and the material constants appeared in the evolution equations

The second part is the identification focused on the determination of the material functions and the material constants appeared in the evolution Eqs. (4.9).

Let us assume that for simplicity we use the scalar internal state variable $\xi = (\boldsymbol{\xi} : \boldsymbol{\xi})^{1/2}$ instead of microdamage tensor $\boldsymbol{\xi}$ and we propose the evolution equation for the porosity ξ as follows

$$\dot{\xi} = \dot{\xi}_{\text{grow}} = \frac{g^*(\xi, \vartheta)}{T_m \kappa_0(\vartheta)} \left[I_g - \tau_{eq}(\xi, \vartheta, \in^p)\right], \tag{4.9}$$

where (cf. DORNOWSKI, PERZYNA [5, 6, 8])

$$
\begin{gathered}
g^*(\xi,\vartheta) = g_1(\vartheta)\frac{\xi}{1-\xi}, \qquad I_g = b_1 J_1 + b_2\sqrt{J_2}, \\
\tau_{\mathrm{eq}}(\xi,\vartheta,\in^p) = a_1(\vartheta)(1-\xi)\ln\frac{1}{\xi}\left\{2\kappa_s(\vartheta) - [\kappa_s(\vartheta)-\kappa_0(\vartheta)]\ F(\xi_0,\xi,\vartheta)\right\}, \\
g_1(\vartheta) = \mathrm{const}, \qquad a_1(\vartheta) = \mathrm{const}, \\
F(\xi_0,\xi,\vartheta) = \left(\frac{\xi_0}{1-\xi_0}\frac{1-\xi}{\xi}\right)^{\frac{2}{3}\delta} + \left(\frac{1-\xi}{1-\xi_0}\right)^{\frac{2}{3}\delta}.
\end{gathered}
\tag{4.10}
$$

As in the infinitesimal theory of elasticity we assume linear properties of the material.

5. Numerical solution of the initial boundary value problem (uniaxial compression)

To integrate our set of nonlinear equations incremental objectivity is achieved by rewriting them in a neutralized configuration. Within the frame of the neutralized configuration the return mapping algorithm is used to solve the system of above equations. All operators are performed at the end of time increment with the corresponding updated rotated stress. We applied our algorithm within ABAQUS/Explicit code by writing a user-material subroutine. To do that we consider the compression quasistatic and dynamic processes (the initial boundary-value problems) for the cylindrical specimen to investigate the deformation mode and to compare the obtained results with those observed experimentally during the processes of direct impact compression test, cf. Jia *et al.* [11], Nemat-Nasser *et al.* [14] and Wang *et al.* [25]. The sample is modeled with 3D solids elements (type C3D8R in the ABAQUS). In numerical simulations the specimen is supported by a transmitting rod and is impacted by a second moving one with an imposed velocity. Both rods in contact with sample are chosen as an elastic bodies with finite friction. Simulation leads to plastic strain and strain rates in the same range as in experimental test of Wang *et al.* [25]. The elasto-viscoplasticity model parameters are determined for specimen with different average grain size for the course grained titanium $d = 30$ μm (CG) and the ultrafine-grained titanium $d = 260$ nm (UFG). In each case we have started our computations assuming at the beginning a broad range of feasible parameters. After initializing and after final determination of material constants which minimising the residua of the constitutive model and the experimental data we apply our model in numerical simulation of uniaxial compression and we have obtain the final state of strain and stress. The mesh of the sample used by finite element code (ABAQUS) and the mesh of the input rot, sample and output rot (element type C3D8R) are presented in Fig. 5a and Fig. 5b. The material constants for pure titanium used in the calculation are listed in Table 1.

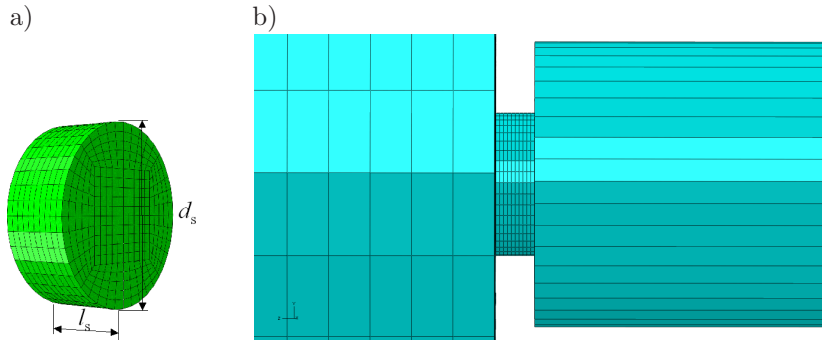

FIG. 5. a) The mesh of the sample used by finite element code (ABAQUS, element type C3D8R). Quasi-static test: $d_s = 3.0$ mm, $l_s = 3.0$ mm; dynamic test: $d_s = 1.5$ mm, $l_s = 0.55$ mm, b) the mesh of the input rot, sample and output rot (element type C3D8R).

Table 1. Material constants for CG titanium.

$\rho_{\mathrm{Ref}} = 4507$ kg/m^3	$E = 110$ GPa	$v = 0.36$	$\vartheta_0 = 296$ K
$\sigma_y^0 = 350.0$ MPa	$\xi_0 = 5 \cdot 10^{-2}$	$\xi_F = 0.2$	$T_m^0 = 5.0$ µs
$g_1 = 1.0$	$b_2 = 1.0$	$c_2 = 1.0$	$n_2 = 1.0$

5.1. Numerical results

Using the elastic moduli and the material parameters for the consolidation mechanism for ncFe powder we have carried out numerical simulations of the true-triaxial tests on iron powder. The simulations are carried out by subjecting a ABAQUS-C3D8R three dimensional elements to uniaxial compression. The Mises stress distribution in the sample for uniaxial compression with initial impact velocity $V_0 = 0.5$ m/s, $d = 260$ nm and $\in^p = 0.20$ is presented in Fig. 6.

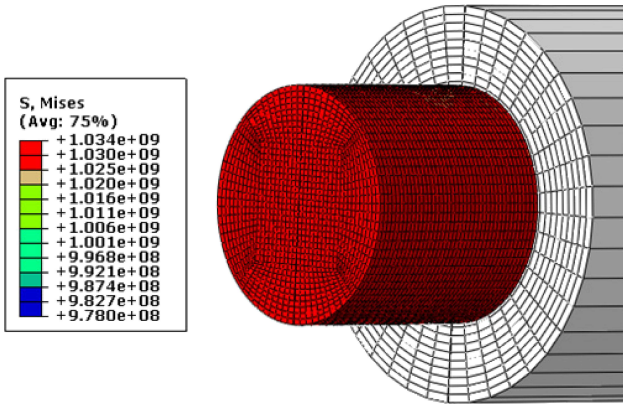

FIG. 6. The Mises stress distribution in specimen obtained by ABAQUS for UFG-Ti ($d = 260$ nm) under quasistatic-strain-rate (1.1–2.2×10^{-3} s^{-1}) uniaxial compression with $V_0 = 0.5$ m/s and $\in^p = 0.1$.

6. Identification of the model

In this section we describe our efforts at determining these material parameters for pure iron powder. The identification of the constitutive models parameters is obtained by an inverse method. The constitutive models require the identification of parameters in view of their application in numerical codes. A parametric identification program is developed, based on a conjugate gradients algorithm. Our objective is to identify the parameters of the viscoplastic constitutive model of Perzyna [21]:

$$\boldsymbol{\beta} = (a,\ b,\ f^0_{SB},\ A,\ B,\ n,\ \dot{\in}^p_s,\ m_2, q,\ g_1,\ b_2,\ c_2,\ n_2).$$

The identification of these constants is carried out by the means of compression true stress-strain diagrams. These curves are generated from the iron experimental tests performed at various strain rates $\dot{\in}^p$ and various average grain sizes d. The proposed model of the grain size dependent viscoplasticity can be completely calibrated by minimising the residua:

$$F(x) = \min \sum_{N_\alpha=1}^{N_\alpha} \frac{\left[\sigma^{\exp}_{\mathrm{eq}}\left(\in^{vp}_\alpha, \dot{\in}^{vp}, d\right) - \sigma^{\mathrm{cal}}_{\mathrm{eq}}\left(\in^{vp}_\alpha, \dot{\in}^{vp}, d, \boldsymbol{\beta}\right)\right]^2}{\left[\sigma^{\exp}_{\mathrm{eq}}\left(\in^{vp}_\alpha, \dot{\in}^{vp}, d\right)\right]^2}, \tag{6.1}$$

where $F(x)$ refers to the residual of the constitutive model and the experimental data with α the experimental number of points and β denotes a vector of unknown material parameters to be determined. Furthermore, $\in^p_\alpha$ are discrete values of the strains $\in^p$. The symbols $\sigma^{\exp}_{\mathrm{eq}}$ and $\sigma^{\mathrm{cal}}_{\mathrm{eq}}$ denote the experimental and calculated stresses for the same strain level $\in^p_\alpha$, N_α is the number of stress-strain data for the test with given strain rate and grain size.

6.1. Identification procedure based on compression tests

To evaluate the quality of the identified parameters, a simulation of compression test is performed on the rectangular sample and compared with the corresponding test. The ABAQUS FEM code was employed to realize this simulation. The sample is modeled with 3D solids elements (type C3D8R in the ABAQUS). In numerical simulations the specimen is supported by a fixed rigid wall and is impacted by a second moving one with an imposed velocity. Rigid walls are chosen as finite planes with finite mass and finite friction. Simulation leads to plastic strain and strain rates in the same range than experimentation. An example of the application of the proposed constitutive description

for modelling of the behaviour of polycrystalline iron under quasistatic and dynamic compression tests for experimental data of JIA *et al.* [11] is depicted in Fig. 7, where the compressive yield strength $\sigma_{\rm eq}^{\rm cal}$ is the equivalent Mises stress.

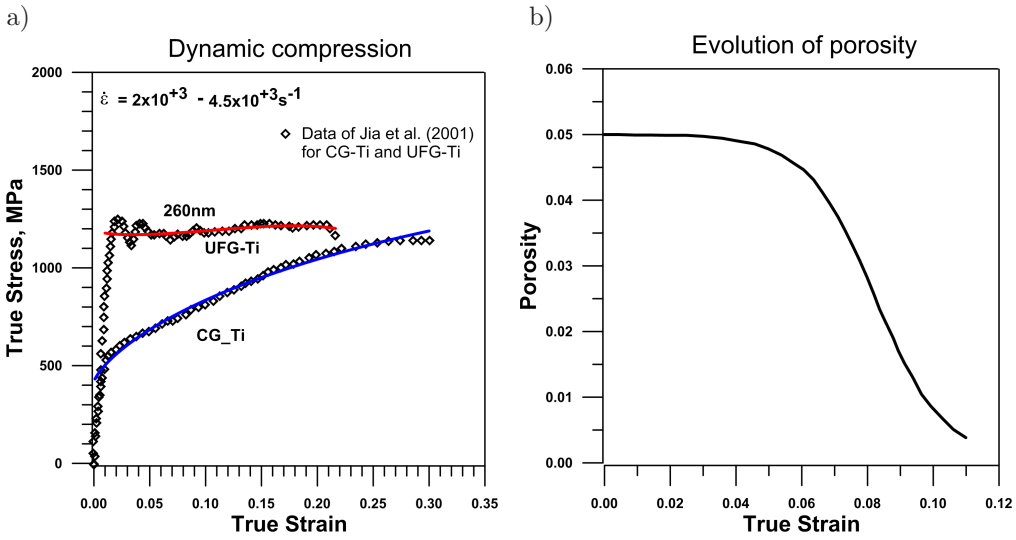

FIG. 7. True stress – true strain for dynamic compression test for titanium from JIA *et al.* [11]. Solid lines represent curves obtained from viscoplasticity model accounting for the shear bands and the evolution of porosity. Symbols ♢ correspond to the dynamic and symbols ♢ correspond to the quasistatic experimental data from JIA *et al.* [11].

Perzyna model parameters are determined for each kind of specimen with different average grain size. In each case we have started our computations assuming at the beginning a broad range of feasible parameters. For instance the initial parameters values in cases for different average grain size: $d = 35$ μm and $d = 260$ nm for dynamic tests which have been taken are presented in Table 2.

Table 2. The initial parameters values for dynamic tests.

$d = 260$ μm	$100.0 \leq A \leq 2000.0$	$5.0 \leq b \leq 1000.0$
	$1.0 \times 10^{+3} \leq \dot{\epsilon}_s^p \leq 1.0 \times 10^{+5}$	$0.01 \leq q \leq 0.5$

We assume some values of our parameters and we start calculations. In case of quasistatic and dynamic compression we use the following forms of Eq. (4.3):

when $d \geq 300$ nm, $f_{SB} = 0$

$$\sigma_{\rm eq}^{\rm cal} = \sigma_{33}^{\rm cal} = \frac{[A(d) + B(\in_\alpha^p)^n]}{\sqrt{1 + n_2\left(\xi_0 + \dfrac{1}{T_m^o}\left(\dfrac{I_g}{\tau_{\rm eq}} - 1\right)^{m_2}\Delta t\right)}} \left(1 + \left(\frac{\left(\dfrac{\dot{\in}^p}{\dot{\in}_s^p(d)} - 1\right)^{m_2}\dot{\in}_\alpha^p}{\dot{\in}_s^p(d)}\right)^q\right) \tag{6.2}$$

when $d \leq 300$ nm, $f_{SB} > 0$ and $n = 0$

$$\sigma_{\rm eq}^{\rm cal} = \sigma_{33}^{\rm cal} = \frac{A^*(d)}{\sqrt{1 + n_2\left(\xi_0 + \dfrac{1}{T_m}\left(\dfrac{I_g}{\tau_{\rm eq}} - 1\right)^{m_2}\Delta t\right)}} \left(1 + \left(\frac{\left(1 - \dfrac{f_{SB}^0}{1 + \exp\left(a - b(d)\in_\alpha^p\right)}\right)\left(\dfrac{\dot{\in}^p}{\dot{\in}_s^p(d)} - 1\right)^{m_2}\dot{\in}_\alpha^p}{\dot{\in}_s^p(d)}\right)^q\right). \tag{6.3}$$

After initializing and after final determination of material constans we apply our model in numerical simulation of uniaxial compression and we have obtain final reaction force and displacement. Now, we can compare our model response with experimental observations.

Finally, the following constitutive parameters are found for the quasi-static and dynamic compression tests when: $d < 300$ nm, $f_{SB} > 0$, $B = 0$, $m_2 = 5.15$, $a = 5$, $f_{SB}^0 = 0.95$, $n_2 = 1$, $b_1 = 0$, $b_2 = 1$, $\xi_0 = 0.05$, $g_1 = 1$, $a_1 = 1$, $\delta = 2.5$ and $n = 0$ (no hardening) and $\boldsymbol{\beta} = (A^*, b, \dot{\in}_s^p, q)$ are presented in Table 3.

Table 3. The identified constitutive parameters for dynamic compression when $d < 300$ nm.

d	$A^*(d)$ [MPa]	b (d)	$\dot{\in}_s^p(d)$ [s^{-1}]	q
260 nm	1187.5	97.5	$3.97 \times 10^{+5}$	0.194

In Fig. 7 solid red lines represent curves obtained from viscoplasticity model accounting for shear bands according to Eq. (6.3). Solid blue lines represent curves obtained from viscoplasticity model without effect of the microshear bands according to Eq. (6.2), symbols $\diamondsuit$ correspond to the dynamic experimental data from Jia *et al.* [11].

6.2. Analysis of the model for low and high strain rates

In Fig. 8 solid red line represents curve obtained from viscoplasticity model accounting for microshear bands according to Eq. (6.3) with $\in^p = 0.06$ and for particular grain size $d = 260$ nm and for entire range of strain rates. Solid blue line represents curve obtained from viscoplasticity model without effect of the microshear bands according to Eq. (6.2) with $\in^p = 0.06$ and for particular grain size $d = 35$ μm and for entire range of strain rates, symbols correspond to the dynamic experimental data from Jia *et al.* [11].

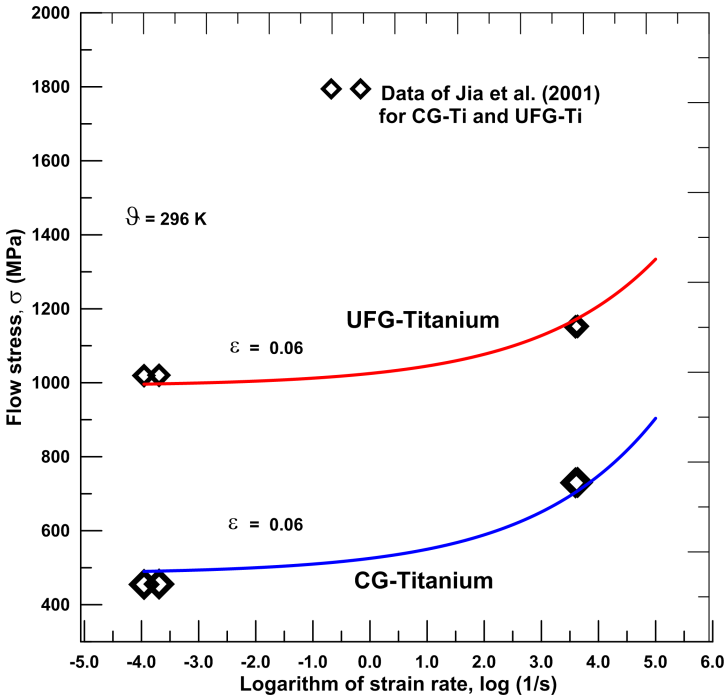

FIG. 8. Flow stress – logarithm of true strain rate for direct compression test of UFG_Ti and CG_Ti for $\varepsilon = 6\%$. Solid lines represent curves obtained from viscoplasticity model accounting the microshear bands and the evolution of porosity. Symbols ♢ correspond to the dynamic and symbols ♢ correspond to the quasistatic experimental data from Jia *et al.* [11].

7. Conclusions

The model has considered the evolution of porosity under the uniaxial impact test. The parameters of model have been identified for titanium under compression within the wide spectrum of strain rates.

In the range of strain rates up to 0.2×10^5 s^{-1} considered, the strength enhancement factor was up to 3. Generally, the experimental results and Perzyna

model predictions for dynamic yield strength values are comparable to each other.

Perzyna overstress model successfully described not only the non-linear rise of flow stress with power strain rate for the case of titanium, but also the upturn of the flow stress at strain rate over about 10^4 s^{-1}.

The proposed description of viscoplastic behaviour of high strength metals, in particular UFG, can be extended accounting for the application of more adequate yield criterion, which in the case of associated flow law, provides also the appropriate potential function.

There is our hope that proposed identification procedure for the thermodynamical theory of elastoviscoplasticity of nanocrystalline metals may be used as a base for the description of the behavior of hexagonal close-packed ultrafine-grained titanium processed by sever plastic deformation and may allow to do the investigation of plastic strain localization and fracture phenomena in nanomechanical processes, for instance compare: Asaro *et al.* [1], Zhu *et al.* [29, 30].

References

1. Asaro R.J., Krysl P., Kad B., *Deformation mechanism transitions in nanoscale fcc metals*, Philosophical Magazine Letters, **83**, 733–743, 2003.

2. Asaro R.J., Needelman A., *Overview no. 42. Texture development and strain hardening in rate dependent polycrystals*, Acta Metallurgica, **33**, 6, 923–953, 1985.

3. Chen M., Ma E., Henker K., *Mechanical behavior of nanocrystalline metals*, [in:] *Nanomaterials handbook*, Y. Gogotsi [Ed.], CRC Press Taylor and Francis Group, pp. 497–529, 2006.

4. Christian J.W., Mahajan S., *Deformation twinning*, Progress in Material Sci., **39**, 1–158, 1995.

5. Dornowski W., Perzyna P., *Constitutive modelling of inelastic solids for plastic flow processes under cyclic dynamic loadings*, Transaction of the ASME, J. Eng. Materials and Technology, **121**, 210–220, 1999.

6. Dornowski W., Perzyna P., *Localization phenomena in thermo-viscoplastic flow processes under cyclic dynamic loadings*, Computer Assisted Mechanics and Engineering Sciences, **7**, 117–160, 2000.

7. Dornowski W., Perzyna P., *Numerical analysis of macrocrack propagation along a bimaterial interface under dynamic loading processes*, Int. J. Solids and Structures, **39**, 4949–4977, 2002.

8. Dornowski W., Perzyna P., *Numerical investigation of localized fracture phenomena in inelastic solids*, Foundation of Civil and Environmental Engineering, **7**, 79–116, 2006.

9. El-Danaf E., Kalidindi S.R., Doherty R.D., *Influence of grain size and stacking-fault energy on deformation twinning in fcc metals*, Metall and Mater Trans. A, **30**, 1223–33, 1999.

10. Gurao N.P., Kapoor R., Suwas S., *Deformation behaviour of commercially pure titanium at extreme strain rates*, Acta Materialia, **59**, 3431–3446, 2011.

11. Jia D., Wang Y.M., Ramesh K.T., Ma E., Zhu Y.T., Valiev R.Z., *Deformation behavior and plastic instabilities of ultrafine-grain titanium*, Applied Physics Letters, **79**, 611–613, 2001.

12. Kumar K.S., Van Swygenhoven H., Suresh S., *Mechanical behavior of nanocrystalline metals and alloys*, Acta Mater., **51**, 5743–5774, 2003.

13. Meyers M.A., Mishra A., Benson D.J., *Mechanical properties of nanocrystalline materials*, Progress in Materials Science, **51**, 427–556, 2006.

14. Nemat-Nasser S., Guo W.G., Cheng J.Y., *Mechanical response and deformation mechanisms of a commercially pure titanium*, Acta Mater., **47**, 3705–3720, 1999.

15. Nowak Z., Perzyna P., *The Identification Procedure for the Constitutive Model of Elasto-Viscoplasticity Describing the Behaviour of Nanocrystalline Iron During Quasistatic and Dynamic Loading Processes*, [in:] Mathematical Methods in Continuum Mechanics, K. Wilmański, B. Michalak, J. Jędrysiak [Eds.], A series of Monographs, Technical University of Lodz, pp. 63–88, 2011.

16. Perzyna P., *Thermodynamic theory of viscoplasticity*, Adv. Applied Mechanics, **11**, 313–354, 1971.

17. Perzyna P., *Constitutive modelling of dissipative solids for postcritical behaviour and fracture*, ASME J. Eng. Materials and Technology, **106**, 410–419, 1984.

18. Perzyna P., *The thermodynamic theory of elasto-viscoplasticity*, Engng. Trans., **53**, 3, 235–316, 2005.

19. Perzyna P., *The thermodynamical theory of elasto-viscoplasticity*, Engineering Transactions, **53**, 235–316, 2005.

20. Perzyna P., *The thermodynamical theory of elasto-viscoplasticity accounting for microshear banding and induced anisotropy effects*, Mechanics, **27**, 25–42, 2008.

21. Perzyna P., *The thermodynamical theory of elasto-viscoplasticity for description of nanocrystalline metals*, Engng. Trans., **58**, 1–2, 15–74, 2010.

22. Pęcherski R.B., *Macroscopic effects of microshear banding in plasticity of metals*, Acta Mechanica, **131**, 203–224, 1998.

23. Pęcherski R.B., *Continuum mechanics description of plastic flow produced by microshear bands*, Technische Mechanic, **18**, 107–115, 1998.

24. Salem Ayman A., Kalidindi Surya R., Doherty Roger D., *Strain hardening of titanium: role of deformation twinning*, Acta Materialia, **51**, 4225–4237, 2003.

25. Wang Y.M., Huang J.Y., Jiao T., Zhu Y.T., Hamza A.V., *Abnormal strain hardening in nanostructered titanium at high strain rates and large strains*, J. Mater. Sci., **42**, 1751–1756, 2007.

26. Wang Y.M., Ma E., *Strain hardening, strain sensitivity, and ductility of nanostructured metals*, Materials Science and Engineering, **A375–377**, 46–52, 2004.

27. Wang Y.M., Ma E., *Three strategies to achieve uniform tensile deformation in nanostructured metal*, Acta Materialia, **52**, 1699–1709, 2004.

28. Wang Y.M., Ma E., Valiev R.Z., Zhu Y.T., *Tough nanostructured metals at cryogenic temperatures*, Adv. Mater., **16**, 328–331, 2004.

29. Zhu B., Asaro R., Krysl P., Bailey R., *Transition of deformation mechanisms and its connection to grain size distribution in nanocrystalline metals*, Acta Mater., **53**, 4825–4838, 2005.

30. Zhu Y.T., Huang J.Y., Ungar T., Wang Y.M., Ma E., Valiev R.Z., *Nanostructures in the Ti processed by severe plastic deformation*, J. Mater. Res., **18**, 1908–1917, 2003.

Received November 21, 2014; revised version December 10, 2014.